Freshwater and heat transports from global ocean synthesis

Article

Published Version

Valdivieso, M., Haines, K., Zuo, H. and Lea, D. (2014) Freshwater and heat transports from global ocean synthesis. Journal of Geophysical Research - Oceans, 119 (1). pp. 394-409. ISSN 0148-0227 doi: https://doi.org/10.1002/2013JC009357 Available at http://centaur.reading.ac.uk/36384/

Published version at: http://dx.doi.org/10.1002/2013JC009357
To link to this article DOI: http://dx.doi.org/10.1002/2013JC009357

Publisher: American Geophysical Union

JOURNAL OF GEOPHYSICAL RESEARCH: OCEANS, VOL. 119, 394–409, doi:10.1002/2013JC009357, 2014

Freshwater and heat transports from global ocean synthesis

M. Valdivieso,[1] K. Haines,[1] H. Zuo,[2] and D. Lea[3]

Received 15 August 2013; revised 19 December 2013; accepted 19 December 2013; published 21 January 2014.

[1] An eddy-permitting 1/4° global ocean reanalysis based on the Operational Met Office FOAM data assimilation system has been run for 1989–2010 forced by ERA-Interim meteorology. Freshwater and heat transports are compared with published estimates globally and in each basin, with special focus on the Atlantic. The meridional transports agree with observations within errors at most locations, but where eddies are active the transports by the mean flow are nearly always in better agreement than the total transports. Eddy transports are down gradient and are enhanced relative to a free run. They may oppose or reinforce mean transports and provide 40–50% of the total transport near midlatitude fronts, where eddies with time scales <1 month provide up to 15%. Basin-scale freshwater convergences are calculated with the Arctic/Atlantic, Indian, and Pacific oceans north of 32°S, all implying net evaporation of 0.33 ± 0.04 Sv, 0.65 ± 0.07 Sv, and 0.09 ± 0.04 Sv, respectively, within the uncertainty of observations in the Atlantic and Pacific. The Indian is more evaporative and the Southern Ocean has more precipitation (1.07 Sv). Air-sea fluxes are modified by assimilation influencing turbulent heat fluxes and evaporation. Generally, surface and assimilation fluxes together match the meridional transports, indicating that the reanalysis is close to a steady state. Atlantic overturning and gyre transports are assessed with overturning freshwater transports southward at all latitudes. At 26°N eddy transports are negligible, overturning transport is 0.67 ± 0.19 Sv southward and gyre transport is 0.44 ± 0.17 Sv northward, with divergence between 26°N and the Bering Strait of 0.13 ± 0.23 Sv over 2004–2010.

Citation: Valdivieso, M., K. Haines, H. Zuo, and D. Lea (2014), Freshwater and heat transports from global ocean synthesis, *J. Geophys. Res. Oceans*, *119*, 394–409, doi:10.1002/2013JC009357.

1. Introduction

[2] Data assimilation is generally known as a method for initializing models with data in order to perform predictions. However, "reanalyses" or syntheses can also use data assimilation to reproduce the historical ocean trajectory, retaining a state close to an historical set of observations being assimilated, *Lee et al*. [2010] and *Stammer et al*. [2010]. In those applications, the recovered ocean circulation and transports of key properties (heat and freshwater) are of great importance. The circulation is needed both to predict future changes in ocean temperatures and atmospheric responses in a forecast, and to infer the contribution/response of ocean advection to past changes in climate. In creating such reanalysis products, the assimilation procedure must also compensate for any drifting of the model away from a realistic trajectory. Several papers have suggested that this effect could be quantified and used to better understand the processes of erroneous drift in models [*Fox and Haines*, 2003; *Rodwell and Palmer*, 2007], and we will examine such diagnostics further.

[3] An ocean synthesis or reanalysis is constructed by assimilating ocean data into a physical model. Generally, the observational data consist of temperature and salinity profiles of the ocean, perhaps in combination with sea level (from satellite altimeters) and satellite sea surface temperatures. The model involved may be entirely dynamical, i.e., geostrophic constraint, or an inverse model where regional budgets are also included using a steady-state assumption, or a fully time evolving general circulation model. In all cases, a key result should be the strength of ocean currents which are otherwise hard to measure, along with the heat and salt/freshwater transports that they carry. With the advent of Argo data (http://www.argo.ucsd.edu; http://argo.jcommops.org), we have large-scale measurements of the ocean salinity field over the past decade, from which the ocean freshwater transports should now be assessed well in ocean reanalyses for the first time.

[4] Although the ocean heat transports have been most frequently assessed, particularly because they are most

[1]National Centre for Earth Observations, Department of Meteorology, University of Reading, Reading, UK.
[2]Now at European Centre for Medium-Range Weather Forecasts, Reading, UK.
[3]UK Met Office, Exeter, UK.

Corresponding author: M. Valdivieso, National Centre for Earth Observations, Department of Meteorology, University of Reading, Whiteknights, PO Box 238, Reading RG6 6AL, UK. (m.valdiviesodacosta@reading.ac.uk)

2169-9275/14/10.1002/2013JC009357

obviously a key climate process, the global freshwater cycle, as well as being important in influencing ocean circulation, is also of critical importance as a key resource for mankind. The terrestrial water cycle has been more extensively studied because of the greater availability of data, however, the oceans cover 71% of the Earth's surface and account for 86% of all evaporation [*Hartmann*, 1994] and 78% of all precipitation [*Adler et al*., 2003], and therefore, air-sea freshwater exchanges and transports within the ocean are of vital importance to understanding the global water cycle. The two main ways of studying the freshwater cycle over the oceans are: (i) using statistical methods for objectively mapping satellite observations and Numerical Weather Prediction (NWP) analyses of air-sea exchanges, e.g., *Yu et al*. [2008] and (ii) using atmospheric reanalysis products to assess air-sea exchanges based on atmospheric transports [see e.g., *Trenberth et al*., 2011].

[5] In the ocean, observations have been less commonly used for freshwater budgets, but when they have they are normally at discrete sections where a scientific cruise makes a snapshot of the temperature and salinity fields, from which geostrophic freshwater transports are calculated. *Wijffels* [2001] provides a summary of such direct estimates of oceanic freshwater transports from ocean hydrographic data and how they compare with indirect estimates based on atmospheric products. *Talley* [2008] presents a global analysis of freshwater transports and their divergences using geostrophic velocities from *Reid* [1994, 1997] and Ekman transports from the National Center for Environmental Predictions (NCEP) R1 reanalysis winds, compared with a global inverse model using hydrographic data [*Ganachaud and Wunsch*, 2003]. *Stammer et al*. [2004] use ocean state estimates for calculating more consistent air-sea exchanges of freshwater, along with heat and momentum exchanges, based on fitting a low-resolution ocean model to a much wider range of nonsynoptic data using long window 4D-Var data assimilation or state estimation methods. The essential element that the ocean model brings is the ability to represent horizontal transports of freshwater, and therefore any ocean reanalysis can be used for assessing freshwater exchanges, not only those calculated using the globally and temporally conservative state estimation methods. Atmospheric reanalyses have been used in this way to assess atmospheric freshwater transports, e.g., *Trenberth et al*. [2011].

[6] In this paper, we study both the ocean freshwater and heat transports in a global 1/4° ocean reanalysis developed during the GMES MyOcean project [*Haines et al*., 2012]. The use of high-resolution modeling and the analysis over the Argo observation period when we have good global salinity measurements for the first time, make this approach new and timely. The paper outline is as follows. A brief summary of the model, the initial conditions and the data assimilation approach are given in section 2. Section 3 discusses the global freshwater budget and the role that ocean data assimilation plays in closing that budget. Section 4 looks at regional freshwater transports and budgets and makes comparisons of meridional freshwater transports from other sources. Section 5 provides discussion and the conclusions.

2. Ocean Reanalysis

[7] We used the Nucleus for European Modelling of the Oceans (NEMO) ocean model, coupled with the Louvain-la-Neuve sea-ice model (LIM2.0) [*Timmermann et al*., 2005; *Goosse and Fichefet*, 1999], with z-levels using hydrostatic and Boussinesq approximations. The model employs a linear free surface [*Roullet and Madec*, 2000] with partial cell topography developed by Mercator Ocean [*Madec*, 2008], based on *Adcroft et al*. [1997], and a tripolar "ORCA" grid at global 1/4° resolution. This reanalysis, which we term UR025.4, is published and available from the British Atmospheric Data Centre (at doi:10.5285/4bcfa3a4-c7ec-4414-863d-caeceb21f16f). UR025.4 uses NEMO version v3.2 with 75 levels in the vertical. The configuration was based on the Drakkar consortium [*Drakkar Group*, 2007] using parameter settings from *Barnier et al*. [2006] and *Penduff et al*. [2010]. Surface atmospheric forcing from the European Centre for Medium-Range Weather Forecasts (ECMWF) ERA-Interim atmospheric reanalysis [*Simmons et al*., 2007; *Dee and Uppala*, 2009; *Dee et al*., 2011] include downward short/long wave radiation, precipitation, 10 m wind, 2 m air humidity, and 2 m air temperature, giving 6 hourly turbulent fluxes calculated from *Large and Yeager* [2004, 2009] bulk formulae. Monthly climatological runoff from *Dai and Trenberth* [2002] is applied along the land mask edge. Unlike many previous modeling studies, no restoration of surface salinity has been used in the UR025.4 reanalysis and, for this reason, the only mechanism restoring surface (and subsurface) salinities is through the increments introduced by data assimilation itself. The model was run for the period 1989–2010 forced with these ERA-Interim data. The results we analyze here are 5 day averages for the last 14 years from 1997 onward. The 5 day data were not stored earlier in the run and this high-frequency output was found later to be necessary to correctly represent freshwater transports in some regions, as will be discussed later. The use of data from 1997 through 2010 also avoids some dynamical spin-up in the early years of the simulation. Applying 3-D data assimilation means that adjustment of the subsurface properties occurs faster than for a surface forced simulation alone, and we found that after the first few years we get reasonably stable estimates of integrated freshwater/heat transports and their divergences. Initial conditions in 1989 are based on an Argo period climatology from the ENhAnced ocean data assimilation and ClimaTe prediction (ENACT/ENSEMBLES) EN3 gridded product (http://metoffice.gov.uk/hadobs/en3), with a cold start from rest.

[8] The assimilation is based on the UK Met Office Forecasting Ocean Assimilation Model (FOAM) operational oceanography assimilation scheme, with a complete description provided by *Martin et al*. [2007], *Storkey et al*. [2010], and references therein. The data assimilation methodology uses analysis correction with multivariate covariances [*Lorenc et al*., 1991] with assimilation increments calculated using a first-guess-at-appropriate-time (FGAT) every 5 days (73 assimilation cycles per year) and introduced evenly over the period in an incremental analysis update (IAU) [*Bloom et al*., 1996] step. UR025.4 assimilates the International Comprehensive Ocean-Atmosphere Data Set (ICOADS) in situ and satellite sea surface temperature (SST) from pathfinder (level 3), and reprocessed Along-Track Scanning Radiometer (ATSR) series data (level 2), similar to the Operational Sea Surface Temperature and Sea Ice Analysis (OSTIA) product in MyOcean v1

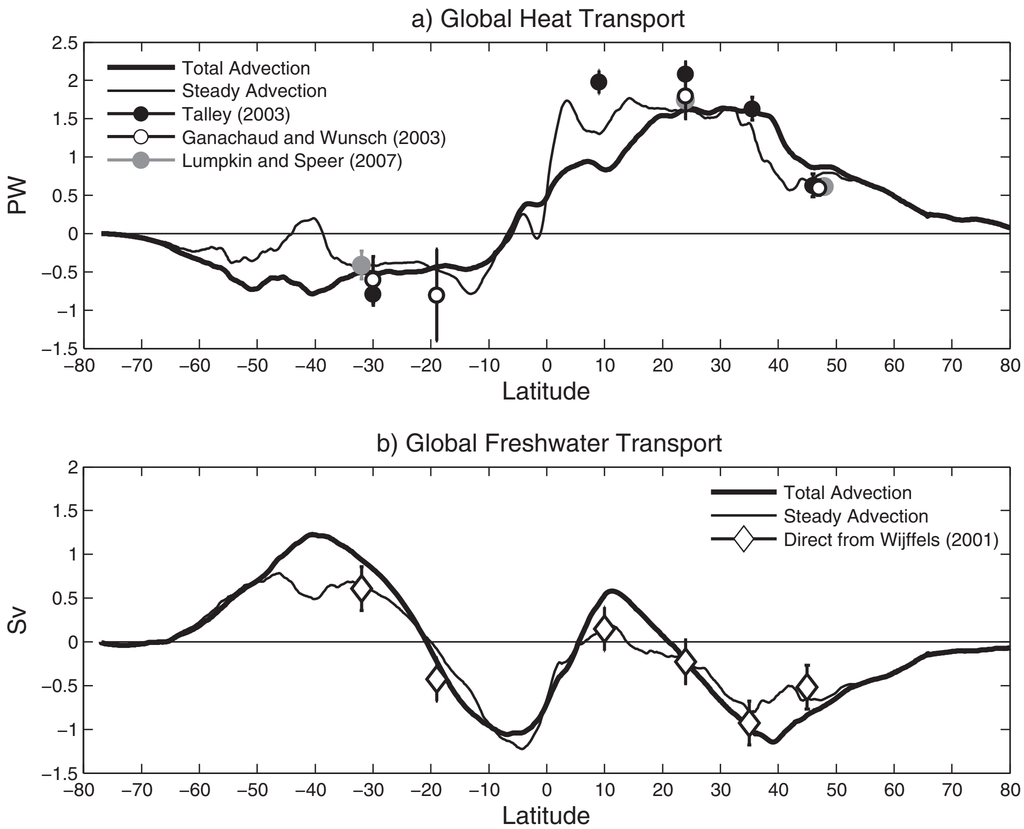

Figure 1. Time-mean (1997–2010) meridional (a) heat and (b) freshwater transport for the global ocean as estimated directly from UR025.4 velocities and temperatures and salinities. Both total transports and steady transports (without eddy correlations, using the 14 year (1997–2010) mean velocities and T, S) are shown. Solid black circles represent estimates from *Talley* [2003] based on *Reid* [1994, 1997] absolute geostrophic velocity analyses for coast-to-coast hydrographic sections and accompanying temperature data. Open black and solid gray circles are WOCE-based inverse model results from *Ganachaud and Wunsch* [2003] and *Lumpkin and Speer* [2007], respectively. The black open diamonds represent direct freshwater transport estimates derived from ocean hydrographic sections compiled by *Wijffels* [2001], who assigned a ±0.25 Sv as the uncertainty in those global estimates. Positive numbers indicate northward transport. Units are in PW and Sv, respectively.

[*Donlon et al*., 2011; *Roberts-Jones et al*., 2012]. Other assimilated data include along-track sea level anomalies from the Collecte, Localisation, Satellites (CLS) Archiving, Validation and Interpretation of Satellites Oceanographic data (AVISO) product (http://aviso.oceanobs.com) assimilated into the model using the *Rio et al*. [2005] Mean Dynamic Topography (MDT), satellite-based sea-ice concentrations from the European Organization for the Exploitation of Meteorological Satellites (EUMETSAT) Ocean Sea Ice Satellite Application Facility (OSI-SAF), and in situ temperature and salinity profile observations from the UK Met Office ENACT/ENSEMBLES EN3_v2a data set, with separate bias correction methods applied for the XBTs [*Levitus et al*., 2009], and for the MDT data [*Lea et al*., 2008].

3. Meridional Transports and Budgets of Heat and Freshwater

[9] The key point of using an ocean data assimilation system is the ability to assess advective transports within and between ocean basins, which can be hard to monitor continuously otherwise. In this section, we first look at the global meridional transports of heat and freshwater and how they compare to independent direct estimates based on ocean hydrographic snapshots, and then look more closely at meridional transports and budgets within the Atlantic basin. We also look at the role of temporal eddy transports at different latitudes.

3.1. Global Meridional Transports

[10] The global meridional transports of heat and freshwater based on reanalysis velocities, temperatures, and salinities, are shown in Figure 1, and are compared at a number of latitudes with prior global estimates, both direct estimates from ocean hydrographic sections [*Talley*, 2003; *Wijffels*, 2001] and inverse model estimations [*Ganachaud and Wunsch*, 2003; *Lumpkin and Speer*, 2007]. Also included for comparison are the transports due to the 14 year (1997–2010) mean velocity advecting the 14 year mean temperature (T) or salinity (S), i.e., without eddy correlations.

[11] There is reasonable agreement between the model's transports and the section-based estimates, but it is interesting to note that at the latitudes where eddy transports are

Table 1. UR025.4 Freshwater Transports at Selected Latitudes of the Global Ocean Averaged Over the Period 1997–2010 Compared to Direct Global Estimates From *Wijffels* [2001][a]

Latitude	UR025.4: Total	UR025.4: Steady	*Wijffels* [2001]
45°N	−0.84	−0.65	−0.52
35°N	−0.99	−0.80	−0.93
24°N	−0.22	−0.20	−0.23
10°N	0.54	0.16	0.15
19°S	−0.22	−0.08	−0.43
32°S	0.94	0.64	0.61

[a]Positive numbers indicate northward transport. Units are in Sv.

strongest (in the subtropics and at the latitude of strong ocean fronts), both the heat and freshwater transports calculated from the time-mean model fields agree more closely with the observational values, particularly for freshwater, than do the full model transports, for example at 32°S, 10°N, and 45°N (see Table 1). Away from the latitudes of the major fronts, and in the subtropics from about 5°N to 15°N, the eddy transports are small. This agrees with results presented in *Stammer*'s [1998] TOPEX/Poseidon eddy analysis and those from high-resolution modeling studies [*McCann et al*., 1994; *Meijers et al*., 2007], which found that eddy freshwater fluxes are small (<0.1 Sv) outside the tropics and the western boundary currents. The significant differences between the total model transports and those mediated by the time mean flows in energetic regions, will be discussed later in more detail when we look at the Atlantic basin.

[12] Figure 2 demonstrates the global balances in meridional heat and freshwater transports relative to the surface forcing and assimilation heat and freshwater sources and sinks. The full meridional advective transports are shown in black (bold lines), along with the integrals of the net surface heat and freshwater fluxes (thin dashed lines), and the assimilation terms (full gray lines), integrated from 80°N southward to the latitude of interest. The assumption here is that the model is near equilibrium or in a quasi-steady state, and that therefore, the integral of the sources and sinks of heat and freshwater should reflect ocean transport across a given latitude band. Clearly for heat transports, there is good agreement between the estimated advective transports and the total sources of heat from the surface fluxes and assimilation terms together (dashed-dotted line), while the air-sea forcing alone does not match the advective transports. However, for the freshwater transports the situation is less clear. Through most of the northern hemisphere, the combined surface and assimilation freshwater

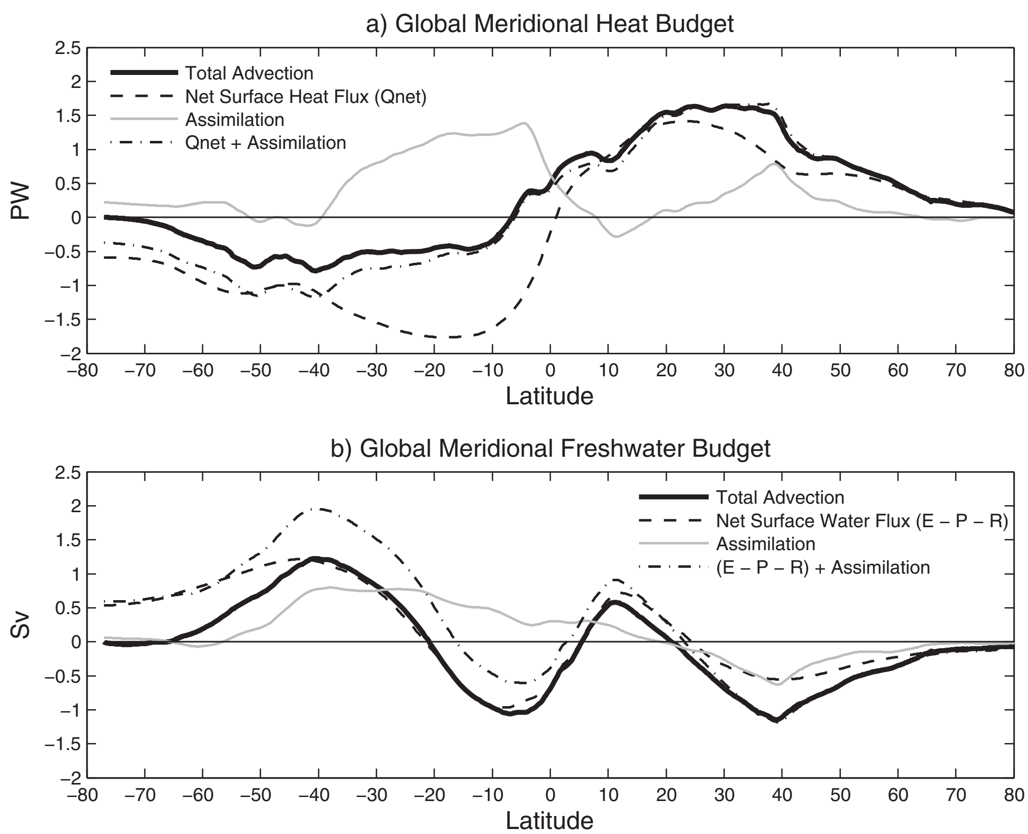

Figure 2. Time-mean (1997–2010) meridional (a) heat and (b) freshwater transport budget for the global ocean, as estimated from reanalysis velocities, temperatures, and salinities, and as inferred from integrated (starting from the north) surface air-sea fluxes and surface fluxes adjusted by data assimilation. Differences between advective transports (bold black line) and those based on air-sea and assimilation fluxes (dashed-dotted line) indicate transient storage of heat and freshwater in the model. Positive numbers indicate northward transport. Units are in PW and Sv, respectively.

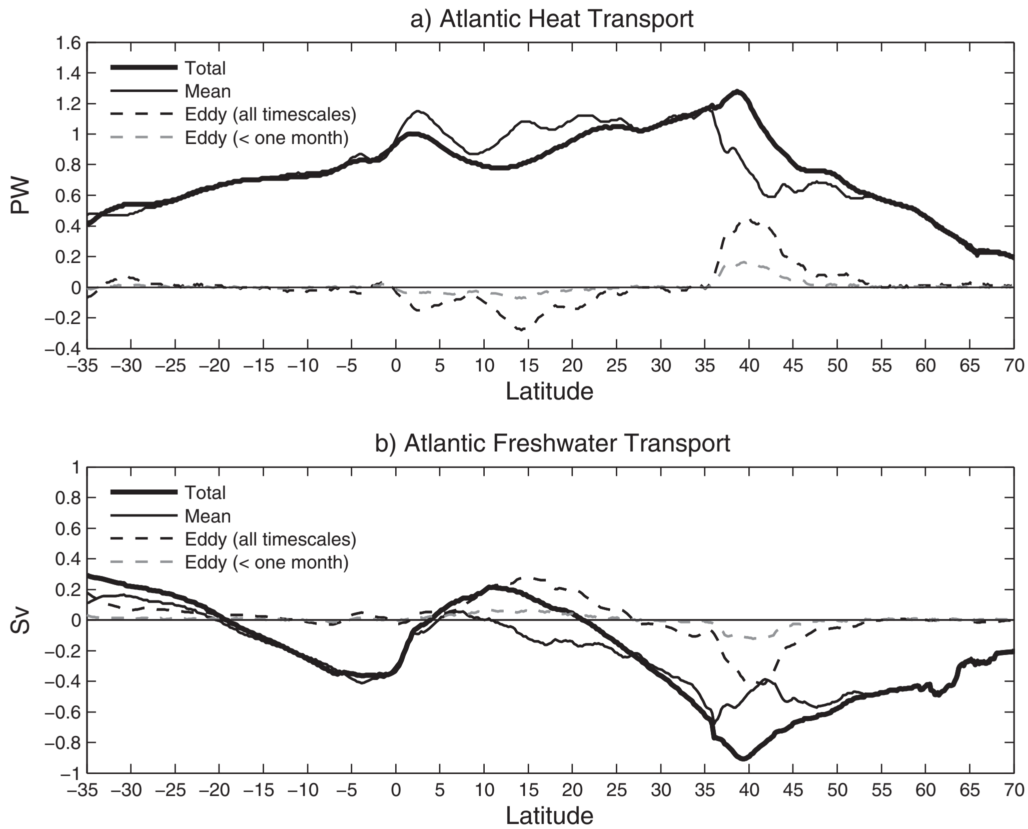

Figure 3. Meridional (a) heat and (b) freshwater transports in the Atlantic in UR025.4 reanalysis over the period 1997–2010. The Total represents advective transport from 5 day mean velocity and (T, S) fields, while the Mean is based on using 14 year mean velocity and (T, S) fields. The two temporal "Eddy" components capture covariability in velocities and (T, S) on all time scales, and only on time scales less than 1 month, respectively. Positive numbers indicate northward transport. Units are in PW and Sv, respectively.

sources match the freshwater transports reasonably well but the curves start to diverge south of ~30°N (note we are integrating freshwater sources southward). We interpret this result as due to a failure of the steady-state assumption over the period 1997–2010, i.e., the source/sinks of freshwater do not match the meridional transports leading to a net trend in freshwater content. This is particularly the case in the South Pacific and Indian basins due to the lack of subsurface observations in the pre-Argo period. Repeating Figure 2 for the shorter period 2005–2010 (not shown) gives a closer balance between source/sinks and meridional transports. We will see later that the Atlantic is in closer steady-state balance. It is interesting that the surface fluxes alone are in relatively good balance with the transports within the Southern Hemisphere down to ~40°S, suggesting that the assimilation terms are compensating entirely for storage changes.

3.2. Meridional Freshwater and Heat Transports in the Atlantic

[13] The meridional exchanges of freshwater in the Atlantic are of particular interest because they reflect export of freshwater from the Arctic, which may change with time due both to climate change (e.g., loss of summer sea ice), and/or changes in freshwater storage in the Beaufort gyre [e.g., *Proshutinsky et al.*, 2002; *Lique et al.*, 2011]. Moving southward, at 48°N freshwater transports are inferred to play an important role in subpolar gyre and Labrador Sea convection, which subsequently helps drive the Atlantic Meridional Overturning Circulation (AMOC) [e.g., *Dong and Sutton*, 2005; *Robson et al.*, 2012]. Freshwater transports by the AMOC are now monitored by the RAPID array at 26°N [*Cunningham et al.*, 2007; E. McDonagh, personal communication, 2013], making this latitude of particular interest for quantitatively testing model based transports. Finally, AMOC-related transports in the south Atlantic may have consequences for the stability of northern overturning circulation and water mass formation that drive the AMOC itself [see e.g., *de Vries and Weber*, 2005; *Drijfhout et al.*, 2010].

[14] Figure 3 shows the Atlantic meridional heat and freshwater transports in the reanalysis. Here, the total transports are decomposed into the sum of a time mean and an eddy component; such that e.g., for the salt transport:

$$\overline{vS}=\overline{v}\,\overline{S}+\overline{v'S'}, \qquad (1)$$

where the overbar denotes a time average (14 years in this case, 1997–2010) and single prime denotes the deviation from that time mean. The eddy transport term, $\overline{v'S'}$, includes variability from the mean on all temporal scales greater than 5 days. Also shown in Figure 3 are the fluxes due to eddy fluctuations on a time scale of less than 1 month. This decomposition is similarly performed for temperature transport.

[15] The transient eddy contributions are substantial on both flanks of the northern subtropical gyre, peaking at around 41°N where mean and eddy transports reinforce each other, with eddy freshwater transport equaling the mean transport, and the eddy heat transport being a little less than the mean transport. Surprisingly, the contribution of eddies on time scales of less than 1 month can reach up to 0.2 PW or 0.1 Sv, corresponding to around 15% of the total transport, showing that, at this 1/4° resolution model, monthly mean model fields are not sufficiently frequent to capture the eddy transport contributions. The contribution from these higher frequency transports is increased by the data assimilation process, because in a similar control model simulation, without any assimilation, the contribution from the submonthly time scale eddy fluctuations reduces to 5% or less of the total transport. However, through the center of the subtropical gyre (e.g., around 26°N where the RAPID array is located) the eddy contributions to transports are always small. The eddy fluxes are transporting heat and freshwater downgradient, with heat being fluxed out, and freshwater being fluxed in, to the subtropical gyre. At around 15°N, it is only the presence of these eddy freshwater fluxes that leads to a region of northward freshwater transport, as the transports from the time mean flow remain southward everywhere north of 20°S. The relative impact of eddies on total heat transports is much less in the band 5°–20°N, because of the large northward heat transports by the mean flow. The meridional distributions of the eddy transports in Figure 3 are qualitatively similar to previous modeling studies, which find maximum eddy transports in the midlatitudes in the Atlantic which act to redistribute heat and salt down the mean gradients [e.g., *Smith et al.*, 2000; *Jayne and Marotze*, 2002; *Treguier et al.*, 2012; *Aoki et al.*, 2013]. Verifying the magnitude of these eddy transports, however, requires further work. *Treguier et al.* [2012] noted an increased northward eddy heat transport (~0.4 PW) at the latitude of the Gulf Stream in a 1/12° resolution run (NATL12), in line with our estimates here, relative to a previous 1/4° control experiment; however, *Smith et al.* [2000] and *Aoki et al.* [2013] found smaller maximum eddy heat transports in the midlatitudes in the Atlantic (<0.15–0.2 PW), from 1/10° resolution models.

[16] It is worth noting that this contribution of eddies of about 0.3 Sv near 15°N (similar in magnitude to the steady component but in the opposite direction) arises mostly from altimetry assimilation, because in a previous reanalysis with only T/S profile assimilation [*Haines et al.*, 2012], eddies give fluxes of less than 0.1 Sv at this latitude. The sea surface height variability from UR025.4 over the period 1993–2010 now has the same amplitude and spatial structure as the AVISO altimetry product across all basins equatorward of 65°N/S, including the tropical Atlantic region discussed above [*Valdivieso et al.*, 2012].

[17] Figure 4 shows how the eddy heat and freshwater transports (over all time scales) are distributed over three model layers: the surface layer from 0.5 m to 97 m, the thermocline layer from 97 m to 947.4 m, and the deep layer from 947.4 m to the bottom. Most of the eddy transport for both heat and freshwater is contained in the depth range from 97 m to 947 m, suggesting that the dynamics that lead to the eddy transport is confined to the thermocline layer. An exception is the surface layer which has a small, but significant contribution for the freshwater transport, order 0.05–0.1 Sv, around 5°–15°N, suggesting covarying velocities and salinity fluctuations within the Ekman/mixed layer.

3.3. Surface Fluxes and Transports in the Atlantic

[18] Following *Wijffels* [2001], mass and freshwater transports through a zonal section in the Atlantic are balanced by the net surface water flux in the area enclosed by the section and the Bering Strait. *Wijffels* [2001, equation (6.2.5)] neglects temporal eddy fluxes (i.e., works from $\overline{v}, \overline{S}$ as in the first component of equation (1)) and assumes a steady state (no ocean storage) to give a freshwater budget expressed as

$$\int\int(P+R-E)dxdy+\int\int Adxdy=\frac{1}{\hat{S}}\int v^{*}S^{*}dxdz+T_{BS}\frac{(S_{BS}-\hat{S})}{\hat{S}} \quad (2)$$

[19] The surface water flux is represented by P (precipitation) + R (runoff) − E (evaporation) (positive into the ocean). $\hat{S}$ is the section averaged salinity, and (v^*, S^*) are the meridional velocity and salinity deviations from the section mean values of $(\overline{v}, \overline{S})$, respectively. T_{BS} is the mean volume transport entering the domain through the Bering Strait (BS), and S_{BS} is the mean salinity at BS (with correlations on the small Bering section assumed negligible). In the case of sequential data assimilation, the left-hand side is incremented by the assimilation source/sink terms, denoted as A. The first term on the right-hand side (RHS) of equation (2) represents the baroclinic freshwater transport across a section in the Atlantic. The second term is the contribution from the Bering Strait throughflow from the Pacific to the combined Arctic/Atlantic ocean. This is also called the "leakage" component and can be interpreted as the salinification of the Bering Strait inflow T_{BS} along its trajectory before reaching the specified section.

[20] Figure 5 shows, for both heat and freshwater, the meridional balances between surface fluxes, assimilation source terms and ocean transports, along with observational estimates from the Atlantic basin. The surface flux and assimilation derived transports assume a steady-state heat and freshwater content and are anchored to the measured transports at 70°N, with the changes calculated by integrating the sources and sinks over areas farther south. Both the total model transports and the steady components are shown. We first note that the total advective meridional fluxes of both heat and freshwater are substantially different from those derived from the model surface fluxes alone. When the surface and assimilation fluxes are considered together, however, they combine to give a good estimate of the mean meridional transports in the model, for both heat and freshwater. Unlike in the global budget shown in Figure 2b, the assimilation freshwater source terms improve the match with the model meridional transports, indicating that the steady-state assumption is more consistent in the Atlantic. In the heat budget, the assimilation terms are

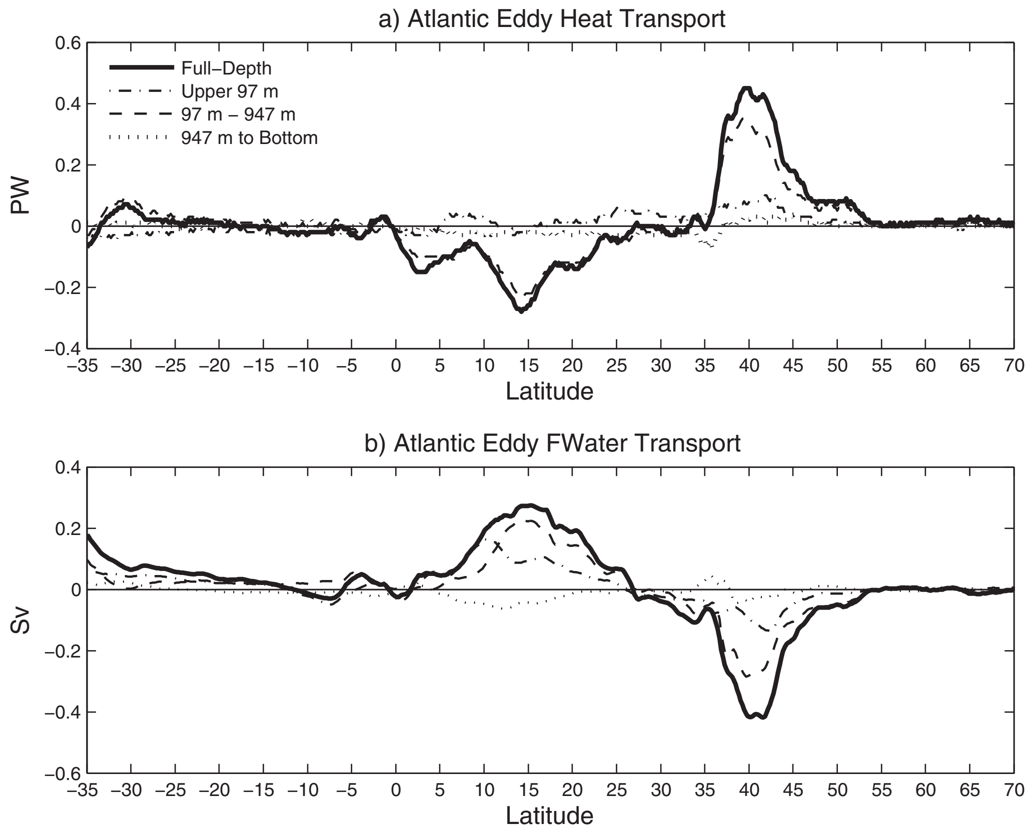

Figure 4. Meridional time-mean (1997–2010) eddy (a) heat and (b) freshwater transports in the Atlantic broken down between the model's surface layer (0.5–97 m), thermocline layer (97–947.4 m), and deep layer (947.4 m—bottom). Positive numbers indicate northward eddy transport. Units are in PW and Sv, respectively.

cooling in the subpolar gyre north of 40°N and warming in the subtropical gyre between 20°N and 40°N, leading to an additional 0.7 PW of heat transport across 40°N into the subpolar gyre. In the equatorial band, the assimilation increments are cooling the model again between 10°S and 10°N, helping maintain around 0.5 PW of northward heat transport through the South Atlantic. This very strong role of data assimilation in maintaining the mean heat content budget is due to the assimilation of SST in the reanalysis, which reduces the need for the bulk sensible heat flux to act to keep SST and surface air temperatures similar [see *Fox and Haines*, 2003]. As in the global ocean, where the meridional heat fluxes by the steady flows differ from the total transports, the observational estimates are more consistent with the steady transports, e.g., for the latitude bands 10°–20°N and 35°–50°N.

[21] Turning to the freshwater transports, the assimilation increments are freshening the ocean north of 40°N, and making the water saltier between 20°N and 40°N, thus tending to reinforce the effect of air-sea fluxes. However, unlike in the heat budget, the freshwater increments (the negative of the salinity innovations) do not make further contributions to the freshwater budget south of 20°N because the assimilation implied transports (gray in Figure 5b) remain constant south of 20°N. Again the freshwater transport by the steady component of the flow generally agrees better with observational estimates of freshwater transport than does the total advective transport, which is consistent with the neglect of the eddies in the Wijffels's analysis.

3.4. Overturning and Gyre Components of the Atlantic Meridional Transports

[22] In order to make comparisons with different components of the section transports, following a number of earlier studies, notably *Bryden and Imawaki* [2001], the mean baroclinic freshwater transport in equation (2) is further decomposed into a mean vertical (or overturning, MOC) component and a mean horizontal (or gyre) component (first and second terms on the RHS) as

$$\frac{1}{\hat{S}}\int v^* S^* dxdz = \frac{1}{\hat{S}}\int \langle v\rangle(z)\langle S\rangle(z)L(z)dz + \frac{1}{\hat{S}}\int \langle v'' S''\rangle dxdz \tag{3}$$

[23] Here, $\langle\cdot\rangle$ denotes the zonal mean, the double prime $''$ indicates deviations from zonal averages, and L is the width of the zonal section as a function of depth. A similar equation can be written for the heat or temperature transport at the section. If we now add back in the time-varying eddy component of freshwater transport, i.e., the temporal correlations of salt and velocity over all time scales from the time mean, the final equation we use to diagnose the total advective depth-integrated freshwater divergence north of a

given Atlantic section relative to Bering Strait (so including the Arctic) is given by equation (4)

$$\text{LHS (equation (2))} = \underbrace{\frac{1}{\hat{S}}\int \langle v\rangle(z)\langle S\rangle(z)L(z)dz}_{overturning\ MOC} + \underbrace{\frac{1}{\hat{S}}\int \langle v'' S''\rangle dxdz}_{gyre} + \underbrace{\frac{1}{\hat{S}}\int \overline{v' S'}\, dxdz}_{eddy} + \underbrace{T_{BS}\frac{(S_{BS} - \hat{S})}{\hat{S}}}_{throughflow} \quad (4)$$

where LHS is the left-hand side of equation (2), i.e., the sum of the surface water flux and the assimiliation source/sink terms. The temporal eddy terms (third component on the RHS) are as defined in equation (1).

[24] Figure 6 shows the Atlantic meridional heat and freshwater transports broken down into the time-mean gyre and overturning components, the time-dependent eddy component, and, for freshwater, the Bering Strait throughflow contribution. The time-mean gyre component of the heat transport plays a role in the South Atlantic between 20°S and the equator, and it starts to be important north of 35°N. The changing roles of gyre and overturning heat transports at the equator, and between overturning transports and eddy fluxes around 35°N, mean that the total northward heat transports vary more smoothly with latitude.

[25] Throughout the northern subtropics, the gyre and MOC components of freshwater transport oppose each other. The peak in southward freshwater transport occurs at around 40°N, just north of the large evaporation zones over the Mediterranean and the subtropical gyre, reaching 0.8 Sv relative to the Bering Strait. The total freshwater transport across 32°S is seen to be ~0.3 Sv equatorward, consistent with atmospheric transports being poleward in midlatitudes. However, the MOC component of the circulation is transporting ~0.1 Sv of freshwater poleward, and indeed the overturning transport is southward at all latitudes in the Atlantic. This southward transport of freshwater by the overturning circulation has been suggested as providing a positive feedback mechanism that could make Atlantic deep water production unstable, e.g., *de Vries and Weber* [2005] and *Hawkins et al*. [2011] (a weakening MOC leads to a fresher Atlantic less susceptible to deep water formation, further weakening the MOC).

[26] There is particular interest in the Atlantic transports at 26°N as these are now being monitored by the RAPID array since April 2004. Table 2 provides estimates for the freshwater transport components across 26.5°N, where the various components are defined according to equations (2) and (3). Also shown for comparison are results from a control experiment with no data assimilated. Time series of the monthly mean freshwater transports at 26.5°N for both the reanalysis and the control are shown in Figure 7. The much stronger temporal variability in the reanalysis run compared to the control is clearly seen, giving potential for higher eddy transports. The eddy term from equation (4) has been incorporated with the gyre component in Figure 7; however, at 26.5°N there is almost no eddy transport in either the control or the reanalysis, and the meridional freshwater transport is achieved entirely by overturning and gyre, mean flows. There is strong variability in both the gyre and overturning components of the freshwater transport, and despite the strong cancelation between these terms in the mean, there is little correlated variability between them (coefficient of −0.17) at this latitude. Given the strong interannual variability in the total transport, it is probably not meaningful to try to define a trend from these values. The throughflow component represents mean transport coming through the Bering Strait (see equations (2) and (4)) and reflects a mean volume transport of 1.4 Sv at a salinity of 32.5 psu (slightly higher than *Aagaard and Cormack* [1989] or the more recent *Woodgate et al*. [2012] observational estimates).

3.5. Basin-Scale Freshwater Divergences Compared to Ocean Direct Estimates

[27] *Wijffels* [2001] derived direct estimates of oceanic freshwater divergences in a number of ocean regions defined by basin-wide hydrographic sections and interbasin fluxes through the Bering and the Indonesian Straits, and compared them with indirect estimates obtained by integrating from north to south the air-sea freshwater flux given by atmospheric reanalysis, and bulk formulae applied to surface observations. *Wijffels* [2001] concluded that systematic errors in bulk parameterizations, but especially in precipitation, of the order of ±0.25 m/yr in the net air-sea flux (which would integrate to 1 Sv over the Pacific basin north of 30°S), gave widely varying indirect transport divergences at the basin scale. In contrast, the ocean transport estimates vary rather less than this, and therefore, they should be used as constraints for generating new air-sea flux products or air-sea parameterization models.

[28] Table 3 shows the model freshwater transports at a number of sections, which can be used to calculate freshwater divergences and budgets for various subbasins. They are presented in terms of contributions from the mean vertical "overturning" and mean horizontal "gyre" components, following the *Bryden and Imawaki* [2001] decomposition (equation (3)), along with an "eddy" transport component which includes all temporal variability, and the Bering Strait (BS) and Indonesian Throughflow (ITF) "leakage" terms. This decomposition of the freshwater transport is shown in equation (4) for sections in the Atlantic.

[29] Table 4 shows total and mean freshwater convergences in the model, based on Table 3, allowing a comparison with *Wijffels*'s direct estimates, as well as the more recent results from *Talley*'s [2008] hydrographic section-based analysis review. We note that both *Wijffels* and *Talley* explicitly neglect temporal correlations of velocity and salinity when using the hydrographic data, and therefore, we expect to see their result match the mean transports derived here.

[30] Starting in the north, in the Arctic and subpolar North Atlantic north of 47°N, there is net convergence including the eddy fluxes of −0.45 ± 0.04 Sv, implying precipitation (here the standard deviations represent interannual variability in the eddy and throughflow contributions). These values are higher than values in *Wijffels* [2001] of −0.25 Sv and *Talley*'s [2008] hydrographic section-based analysis of −0.32 Sv for the Atlantic/Arctic north of 45°N, but still within the range of the uncertainties

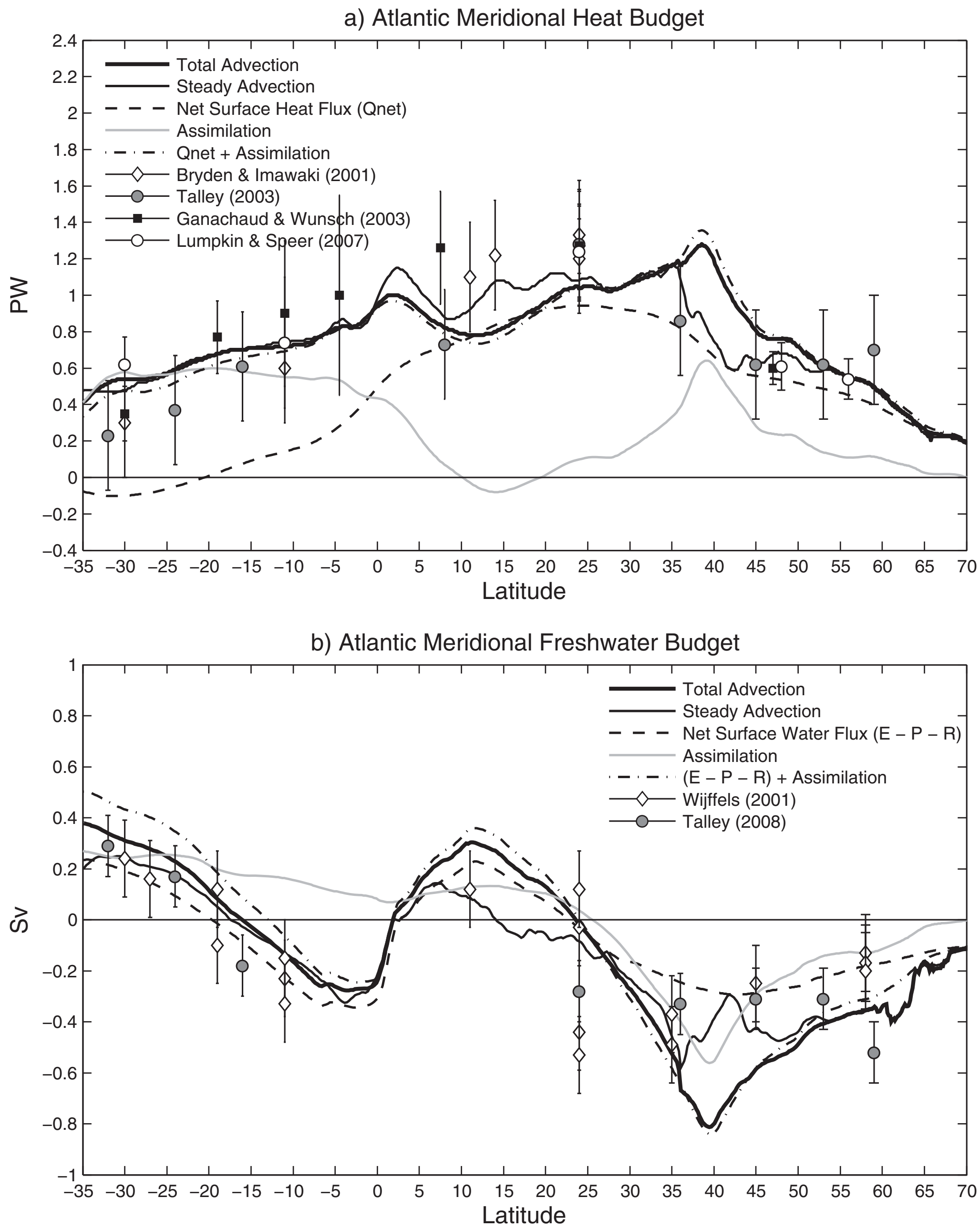

Figure 5. Total (a) heat and (b) freshwater transport divergences north of the zonal sections in the Atlantic and the Bering Strait, along with the source/sink implied transports based on a steady-state assumption through the period 1997–2010. As the net surface heat (Qnet) and freshwater (E − P − R) fluxes do not take into account the transports entering the domain via the Bering Strait, the advective transports of heat and freshwater at 70°N have been added to the surface fluxes to allow the comparison. The surface heat and freshwater fluxes alone clearly do not imply consistent meridional transports, but when the Assimilation terms are included the match with the observed transports is very close. The observational transport estimates at various sections are also included for comparison. Positive represents ocean heating and net evaporation in the region. Units are in PW and Sv, respectively.

associated with those direct estimates of ±0.17 to ±0.3 Sv, as reported by *Wijffels* [2001].

[31] The implied net precipitation/runoff in the north Pacific north of 47°N is −0.18 ± 0.02 Sv, which lies between the estimates in *Wijffels* [2001] (−0.27 Sv) and *Talley* [2008] (−0.11 Sv). If a larger North Pacific region is examined, from 24°N to Bering Strait, the implied precipitation/runoff is −0.28 ± 0.04 Sv, again in line with *Wijffels*'s [2001, Table 6.2.2], in the range of −0.21 to −0.29 Sv.

[32] The Atlantic/Arctic total convergence of 0.33 ± 0.04 Sv (net evaporation) north of 32°S is made up

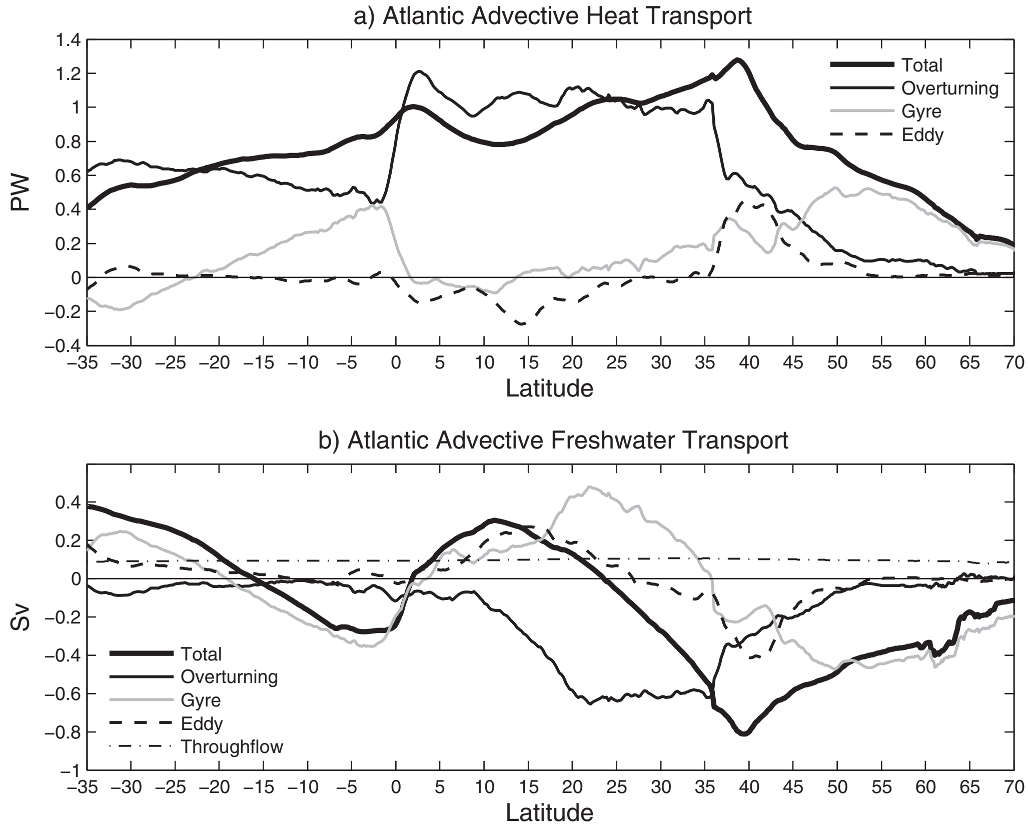

Figure 6. Time-mean (1997–2010) meridional (a) heat and (b) freshwater transports associated with the mean "Overturning", mean "Gyre," and "Eddy" components, and the BS "Throughflow" contribution (in the case of freshwater transport, see equation (4)). These components (positive northward) are additive parts of the "Total" transport divergence north of a given latitude band in the Atlantic relative to BS. Positive is ocean heating or net evaporation in the region. Units are in PW and Sv, respectively.

of several contributions shown in Table 3, including the freshwater import from the Southern Ocean via the mean gyre (0.25 Sv) and through the Bering Straits (0.09 ± 0.01 Sv), along with a southward overturning transport of −0.11 Sv associated with export of north Atlantic deep water to the Southern Ocean, and a flux of <0.1 Sv from the eddies. The convergence of the time mean flux at 0.23 ± 0.01 Sv compares extremely well with *Wijffels* [2001] and *Talley* [2008] for the same region of 0.24 Sv and 0.28 Sv, respectively, although the total convergence including the eddy terms is rather larger, again showing direct estimates comparing better to mean transports in the model.

[33] The Pacific Ocean north of the 32°S has weak convergence by the mean flow alone of 0.03 ± 0.03 Sv, composed of freshwater import from the Southern ocean via the mean horizontal gyre (0.27 Sv), offset by freshwater export by the mean overturning (−0.06 Sv), flow to the Atlantic through the Bering Strait (−0.08 ± 0.01 Sv) and export to the Indian basin through the Indonesian throughflow (−0.10 ± 0.03 Sv). This again agrees with the estimates

Table 2. Time Mean Advective Freshwater Transports in the Atlantic at 26.5°N From UR025.4 and Control (With No Data Assimilation) and Their Monthly Standard Deviations for Two Periods: One is the Last 14 Years From 1997 to 2010, and the Other Is the Period From April 2004 to December 2010, Overlapping With the RAPID Array[a]

	UR025.4		Control	
Freshwater Transport	1997–2010	Apr 2004–Dec 2010	1997–2010	Apr 2004–Dec 2010
Total	−0.11 ± 0.23	−0.13 ± 0.23	−0.08 ± 0.12	−0.05 ± 0.13
Overturn	−0.64 ± 0.18	−0.67 ± 0.19	−0.38 ± 0.12	−0.35 ± 0.13
Gyre	0.42 ± 0.18	0.44 ± 0.17	0.19 ± 0.04	0.20 ± 0.05
Throughflow	0.10 ± 0.04	0.10 ± 0.04	0.10 ± 0.04	0.10 ± 0.04

[a]The Total fluxes are calculated from the sum of the monthly mean Overturning, Gyre, and Throughflow flux components. Note that temporal eddy transports are insignificant at this latitude, but would conventionally be included with the gyre terms. Positive numbers indicate northward transport. Units are in Sv.

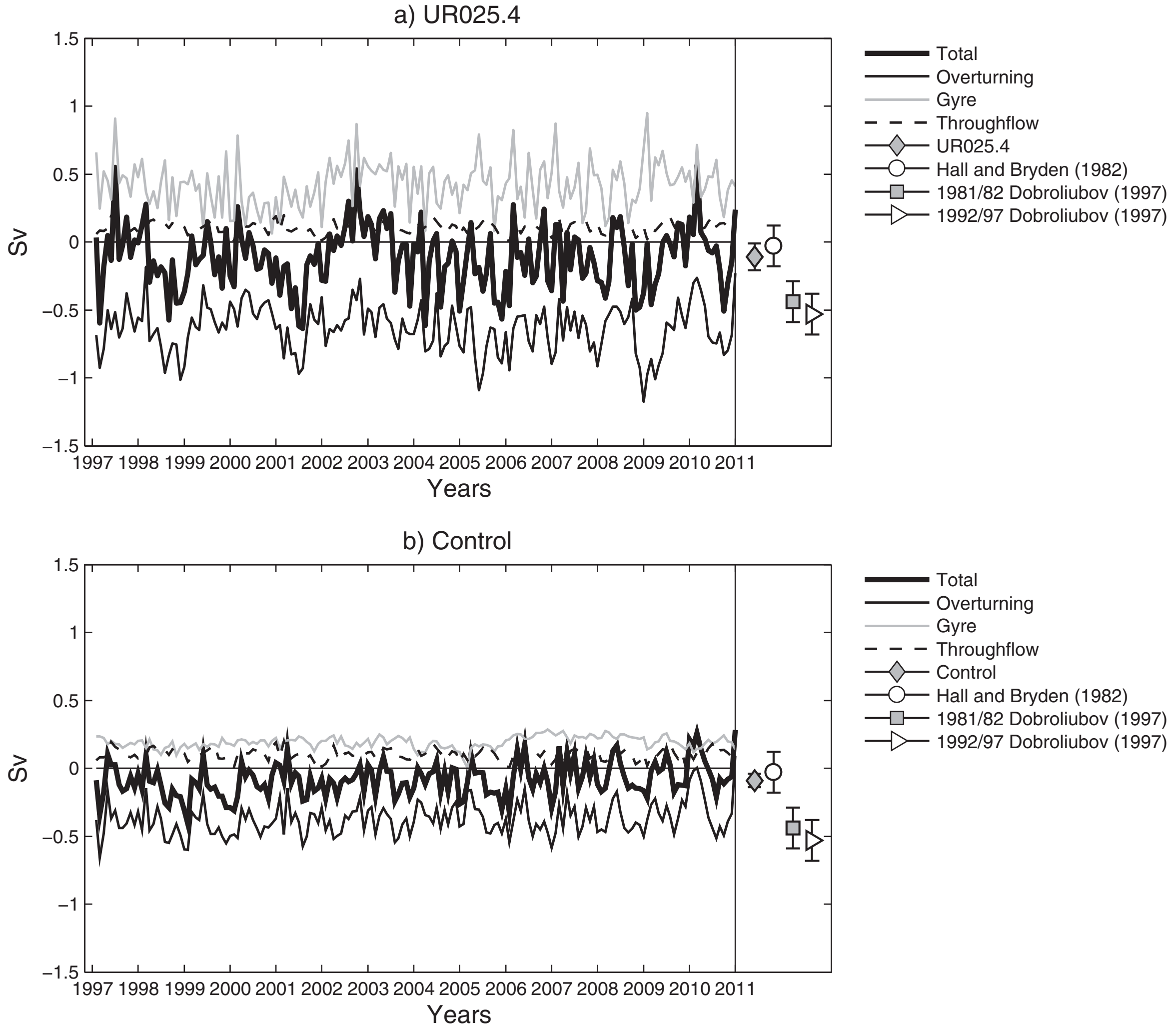

Figure 7. Time series of the monthly Atlantic freshwater transports at 26.5°N from the UR025.4 reanalysis and from the control run simulation with no data assimilation. Symbols on the right-hand side represent observational transport estimates from *Wijffels*'s [2001, Table 6.2.2]. At this latitude, eddy correlations are negligible (see Figure 3) and have been included in the horizontal ("Gyre") component. Units are in Sv.

reported in *Wijffels* [2001] in the range of 0.06–0.09 Sv for net evaporation, and *Talley* [2008] of -0.04 ± 0.10 Sv, i.e., with close to zero net precipitation/evaporation throughout the Pacific north of 32°S. The total convergence (implied evaporation), including eddies, increases however to 0.09 ± 0.04 Sv, so again the agreement with the mean transports alone is a little better.

[34] For the Indian Ocean north of 32°S, there is convergence (implied net evaporation) of 0.49 ± 0.03 Sv without the eddy contribution (or 0.65 ± 0.07 Sv including eddy fluxes). More moderate estimates are reported in *Wijffels* [2001] of around 0.31 Sv and *Talley* [2008] of 0.38 Sv, whereas a larger net loss of 0.58 Sv, more comparable to this study, is obtained by *Ganachaud and Wunsch* [2003] from a WOCE-based inverse model, and also by *Schanze et al*. [2010], based on air-sea flux products. The mean flow transports across 20°S in the Indian Ocean are in better agreement with the observations, although contributions from eddies are still substantial. We would of course expect a priori that products based in some way on surface fluxes would agree better with the total section transports rather than with transports by the mean flow alone. The large net evaporation calculated here is dominated by the freshwater import from the Southern Ocean via the mean gyre circulation (0.52 Sv), with a smaller contribution from the Indonesian Throughflow of 0.1 Sv. However, in this region eddies make up over 30% of the total northward freshwater transport across 32°S, mostly occurring in the southwest Indian Ocean sector of the Antarctic Circumpolar Current (ACC).

[35] If we integrate across the whole Southern Ocean boundary at 32°S, the model exports a substantial amount of freshwater from the Southern Ocean (1.07 Sv). However, if we only consider the transports by the mean flow, this drops to 0.74 Sv, which is again much closer to the values reported in *Wijffels* [2001] and *Talley* [2008] of around 0.6 Sv south of 30°S. The largest discrepancies with the observations, based on both the mean flow transports and the eddy transport contributions, come from the Indian Ocean sector.

Table 3. Section/Time-Averaged Salinity (psu) and Time Mean Freshwater Transport Components (Sv) Over the Period 1997–2010 at a Number of Basin-Wide Sections[a]

Section	Section-Averaged Salinity	(1) Mean Overturning	(2) Mean Gyre	(3) Eddy (All Scales)	(4) Mean Section Transport (1) + (2)	(5) Total Section Transport (1) + (2) + (3)	(6) BS Component	(7) ITF Component	(8) Mean Convergence (4) + (6) + (7)	(9) Total Convergence (5) + (6) + (7)
Atl 47°N	35.01 ± 0.01	−0.11	−0.38	−0.06 ± 0.03	−0.49	−0.54 ± 0.03	0.10 ± 0.01		−0.39 ± 0.01	−0.45 ± 0.04
Pac 47°N	34.46 ± 0.00	−0.05	−0.03	−0.02 ± 0.01	−0.08	−0.10 ± 0.01	−0.08 ± 0.01		−0.16 ± 0.01	−0.18 ± 0.02
Atl 35°N	35.23 ± 0.01	−0.63	0.09	−0.05 ± 0.05	−0.54	−0.60 ± 0.05	0.11 ± 0.01		−0.44 ± 0.01	−0.49 ± 0.06
Pac 35°N	34.54 ± 0.00	0.01	−0.26	−0.12 ± 0.02	−0.24	−0.36 ± 0.02	−0.08 ± 0.01		−0.32 ± 0.01	−0.44 ± 0.03
Atl 26.5°N	35.18 ± 0.00	−0.67	0.40	0.03 ± 0.02	−0.26	−0.23 ± 0.02	0.10 ± 0.01		−0.16 ± 0.01	−0.13 ± 0.03
Pac 24°N	34.59 ± 0.00	−0.05	−0.07	−0.08 ± 0.03	−0.12	−0.19 ± 0.03	−0.08 ± 0.01		−0.20 ± 0.01	−0.28 ± 0.04
Atl 16°S	34.90 ± 0.00	−0.03	−0.13	0.02 ± 0.02	−0.16	−0.14 ± 0.02	0.09 ± 0.01		−0.07 ± 0.01	−0.04 ± 0.03
Ind 20°S	34.75 ± 0.00	−0.05	0.05	0.09 ± 0.05	0.0	0.10 ± 0.05		0.10 ± 0.03	0.10 ± 0.03	0.20 ± 0.06
Pac 17°S	34.71 ± 0.00	0.03	−0.18	−0.02 ± 0.05	−0.16	−0.17 ± 0.05	−0.09 ± 0.01	−0.10 ± 0.03	−0.34 ± 0.03	−0.36 ± 0.06
Atl 32°S	34.80 ± 0.00	−0.11	0.25	0.09 ± 0.04	0.14	0.24 ± 0.04	0.09 ± 0.01		0.23 ± 0.01	0.33 ± 0.04
Ind 32°S	34.69 ± 0.00	−0.13	0.52	0.17 ± 0.06	0.39	0.55 ± 0.06		0.10 ± 0.03	0.49 ± 0.03	0.65 ± 0.07
Pac 32°S	34.63 ± 0.00	−0.06	0.27	0.07 ± 0.03	0.21	0.28 ± 0.03	−0.08 ± 0.01	−0.10 ± 0.03	0.03 ± 0.03	0.09 ± 0.04

[a]Positive is northward transport. Annual Eddy fluxes (±1STD) are listed in the fifth column; annual freshwater convergences (Sv) north of a given section are given in the last two columns of the table. Positive represents implied net evaporation.

4. Closing the Basin Freshwater Budgets

[36] Up to now we have focussed on inferences from the diagnosed transports in the ocean reanalysis because this is what is being geostrophically constrained most by the assimilation of water properties. However, connecting those transports to air-sea fluxes necessarily assumes that the model is in steady-state conditions. In this section, we look at closing the budgets for the model, particularly for the freshwater budget.

[37] As Table 1 of *Schanze et al*. [2010] shows the global freshwater budgets from Atmospheric reanalyses are not generally well balanced, with discrepancies for ERA products for example, up to 2 Sv or more. We have computed the model's depth-integrated freshwater budget over the period 1997–2010. Terms in the budget are shown as a function of latitude and longitude in Figure 8, and they include:

[38] 1. Figure 8a: Transient storage of full-depth freshwater content (relative to 35 psu), Ftend.

[39] 2. Figure 8b: Freshwater transfer across the ocean surface, Fsurf, evaporation/precipitation and runoff.

[40] 3. Figure 8c: Convergence of freshwater through the vertically integrated horizontal flow, Fadv, including eddies.

[41] 4. Figure 8e: Freshwater source/sinks, Fassim, associated with vertically integrated salinity increments.

[42] 5. Figure 8f: Residual fluxes, Fres, calculated from the sum of all terms.

[43] Storage of freshwater (Figure 8a), represented by the trend in full-depth freshwater content relative to 35 psu, is mostly insignificant compared to the net surface water flux (Figure 8b) and the divergence freshwater transports (Figure 8c). Assimilation fluxes (the negative of the depth-integrated salinity increments in Figure 8e) indicate that salinity observations may have a local impact comparable with the surface freshwater flux itself. The large fluxes here are generally associated with correcting the position and scale of strong narrow fronts, such as western boundary currents and the ACC. The residual of the four-term balance, Ftend − Fsurf − Fadv (advective fluxes including eddy correlations) − Fassim (Figure 8f), mainly represents subgrid scale processes due to horizontal mixing, and is small when compared with the other terms, except in regions of strong T/S gradients such the western boundary currents and the ACC. Also shown in Figure 8d is the eddy convergence of the freshwater transport due to temporal correlations of salinity and velocity over all time scales from the 14 year mean. The Atlantic and the Indian basins, and the Indian sector of the ACC are important regions of eddy freshwater convergence or divergence, while the subtropical gyres in the Pacific are mostly regions of strong mean flow convergence, seen by comparing Figures 8c and 8d.

[44] Freshwater balances for the global ocean and for each basin are given in Table 5, with basin boundaries outlined in Figure 8a, highlighting basin-to-basin differences in freshwater budgets, with the southern ocean boundary defined at 32°S, and the Atlantic/Arctic boundary defined along the tripolar ORCA grid close to 70°N. The Atlantic basin then includes Hudson Bay and the Baltic, Mediterranean and Black Seas. The boundary between the Indian and

Table 4. Comparison of Freshwater Convergences (Sv) From UR025.4 Reanalysis Over the Period 1997–2010 With Direct Estimates From Ocean Hydrographic Sections Compiled by *Wijffels* [2001, Table 6.2.2], and *Talley*'s [2008] Hydrographic Section-Based Analysis[a]

Freshwater Convergence	Hydrographic Section-Based		UR025.4	
	Wijffels [2001]	*Talley* [2008]	Mean	Total (Including Eddies)
Arctic/Atlantic				
45°–47°N to Bering	−0.25	−0.32	−0.39	−0.45 ± 0.04
35°N to Bering	−0.37	−0.33	−0.44	−0.49 ± 0.06
24°–26°N to Bering	+0.12	−0.29	−0.16	−0.13 ± 0.03
16°–19°S to Bering	−0.10	−0.18	−0.07	−0.04 ± 0.03
North of 30°–32°S	+0.24	+0.28	+0.23	+0.33 ± 0.04
Indian				
North of 20°S	−0.03	+0.07	+0.10	+0.20 ± 0.06
North of 32°S	+0.31	+0.38	+0.49	+0.65 ± 0.07
Pacific				
47°N to Bering	−0.27	−0.11	−0.16	−0.18 ± 0.02
35°N to Bering	−0.56	−0.15	−0.32	−0.44 ± 0.03
24°N to Bering	−0.21	−0.19	−0.20	−0.28 ± 0.04
17°S to Bering	−0.30		−0.34	−0.36 ± 0.06
32°S to Bering	+0.06	−0.04	+0.03	+0.09 ± 0.04

[a]The total transports (last column) include eddies and the ±values represent annual standard deviations over the 14 year period. Positive is implied net evaporation; negative is implied net precipitation/runoff.

Pacific follows the model grid across the Indonesian passages.

[45] The global budget shows a change in storage through the period with the ocean getting slightly saltier by the equivalent of 0.34 Sv, with equal contributions from the Atlantic and Pacific basins. Assimilation is contributing only a small part to this change with most of it coming from net evaporation at the surface. At the basin scale, the Atlantic and the Indian oceans show up clearly as evaporation basins, the Pacific has an almost closed freshwater budget, consistent with the model section-based estimates shown previously in Table 4, while the Arctic and Southern oceans show net precipitation. Only the Arctic shows relatively small contributions from assimilation, probably because of the lack of observational data. Elsewhere the net assimilation contributions are strong and have the same sign as the surface flux terms, with the sum of the surface forcing and assimilation balancing the advective transports for each basin. The assimilation also has the same sign as the storage, perhaps indicating storage changes directly introduced by assimilating Argo during the reanalysis period. The residual terms are generally smaller than most other terms for all basins, and represent transport errors due to mixing, particularly in regions of strong temperature/salinity gradients such the western boundary currents and the ACC. (This table can also be compared to *Haines et al.* [2012], where the budgets for an earlier NEMO reanalysis, using an older model version with only profile assimilation, were shown).

5. Summary and Discussion

[46] We have analyzed the heat and freshwater transports in a 20 year global ocean reanalysis based on the NEMO $^1/_4$° ocean model and compared the results with observations from independent hydrographic sections. We have also looked at how these transports are maintained through surface fluxes and data assimilation and looked at the contribution of temporal eddy transports. One of the key findings is that the role of temporal eddy transports can be substantial at certain latitudes, and that where this occurs, the match with previous observation-based transports is more consistent with the transports mediated by the time mean flows in the model. Eddy transport correlations on time scales of less than 1 month can even be substantial at some latitudes.

[47] We found that ocean data assimilation substantially increases the temporal variability of meridional mass transports (Figure 7), and that at some latitudes this leads to considerably stronger eddy heat and freshwater transports compared to model simulations without data assimilation. It is well known that a free run of a $^1/_4$° ocean model will generally under-represent eddy activity at all latitudes, e.g., in comparison to altimeter measured sea level variability, and the assimilation here increases the eddy variance to be consistent with observations. The resultant increase in transports also reflects the stronger frontal gradients maintained through data assimilation. In reality these gradients are usually maintained by mean flow transports and by the frontogenesis caused by the eddies themselves. Further work with transport comparisons to both a control run and higher resolution model simulations with more realistic eddy variances, would be useful to help understand how this process operates within a reanalysis run.

[48] The assimilation affects regional and global heat and freshwater budgets in two ways. In the heat budget, there are strong feedbacks between sea surface temperatures and sensible and latent heat fluxes, so that assimilation of SST observations will directly influence the terms in the bulk formulae used for modeling the air-sea fluxes. A second indirect impact comes from using assimilation increments to update the ocean properties. These increments ensure that any remaining inconsistencies between surface fluxes and the ocean full-depth transport convergences can be reconciled by assimilation sources and sinks. We show that air-sea forcing and assimilation terms

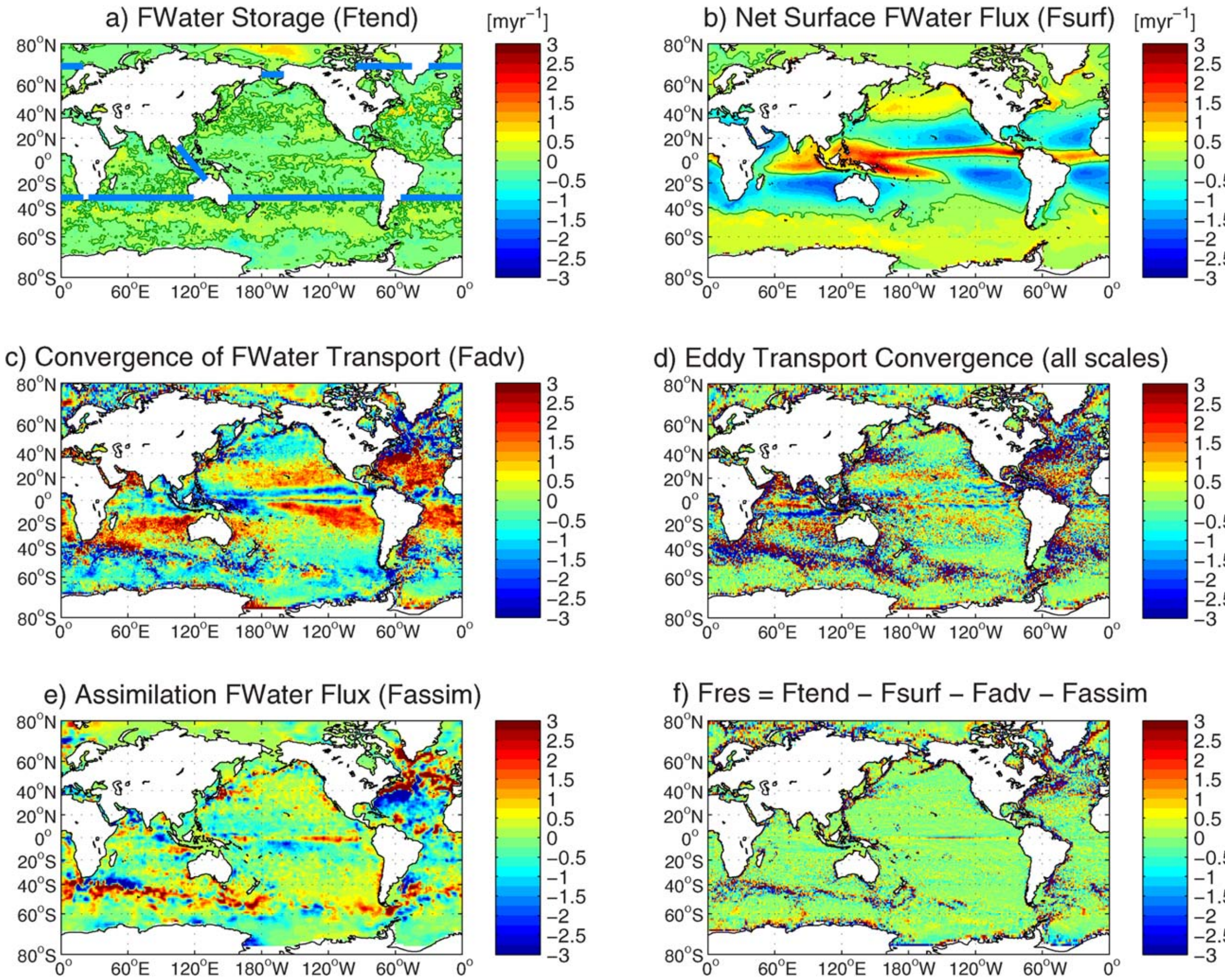

Figure 8. Depth-integrated freshwater budget (units in m/yr) over the period 1997–2010. Here, Ftend, Fsurf, Fassim, Fres, and Fadv (the total freshwater convergence including the eddy convergences plotted separately in plate (d) for comparison) are positive when they act to increase the full-depth freshwater content relative to a reference salinity of 35 psu (i.e., implied net precipitation and runoff). Also shown in Figure 8a are the boundaries for the ocean basins used in the budget analysis listed in Table 5.

together then provide a close balance to the advective convergence or divergence of heat and freshwater by the vertically integrated circulation. The fact that the mean flow component of the reanalysis transports also match independent observation-based estimates of the time mean heat and freshwater transports in all ocean basins, is taken as a good indication that the assimilation sources are not distorting these transports. We also looked in the Atlantic basin at the time mean overturning and gyre components, along with the temporal eddy transports for heat and freshwater, deriving transports that can be compared with the 26°N Rapid array values for example.

[49] The strong eddy transports identified at some latitudes in this reanalysis require further work to independently verify. Although the *Wijffels* [2001] and *Talley* [2008] freshwater transports explicitly neglect eddy

Table 5. Annual Mean Freshwater Balances for Each Ocean Basin (See Basin Boundaries in Figure 8a) Over the Period 1997–2010[a]

Region	Surface Area (m^2)	Advection (Fadv)	Air-Sea Flux (Fsurf)	Assimilation (Fassim)	Storage (Ftend)	Residual (Fres)
Arctic	1.23e+13	−0.11 ± 0.03	0.14 ± 0.00	0.02 ± 0.06	0.02 ± 0.07	−0.03 ± 0.01
Atlantic	6.87e+13	0.47 ± 0.05	−0.36 ± 0.10	−0.30 ± 0.96	−0.17 ± 0.95	0.02 ± 0.10
Indian	4.31e+13	0.48 ± 0.04	−0.36 ± 0.10	−0.19 ± 0.25	−0.05 ± 0.26	0.01 ± 0.04
Pacific	1.35e+14	0.13 ± 0.05	−0.03 ± 0.24	−0.28 ± 0.47	−0.18 ± 0.36	0.00 ± 0.04
Southern O.	1.02e+14	−0.96 ± 0.07	0.36 ± 0.05	0.68 ± 0.67	0.04 ± 0.64	−0.04 ± 0.05
Global	3.61e+14	0.00 ± 0.00	−0.24 ± 0.40	−0.07 ± 1.45	−0.34 ± 1.25	−0.04 ± 0.15

[a]The residual of the balances, Fres = Ftend − Fadv (including eddy correlations) − Fsurf – Fassim, is listed in the last column. Positive is net precipitation and runoff, negative is net evaporation. The ± values represent annual standard deviations over the 14 year period. Units are in Sv.

correlations, it should be noted that even single hydrographic section analyses might easily underrepresent important eddy transports. The spatial sampling along hydrographic sections tends to be typically 50–100 km at best, which will only sample eddy correlations on larger scales, particularly, because additional spatial smoothing is needed to calculate normal property transports. Eddies will often be confined to some fraction of a trans-ocean section, and the region where eddy transports are important may be further confined to regions where the eddies are growing baroclinically. Further analysis of our reanalysis results (not shown) suggest that these smaller subsections would need to be especially well sampled hydrographically to capture the eddy correlations correctly, and this would be a good topic for investigation with higher resolution models.

[50] The key products of this high-resolution reanalysis are the advective transports of heat and freshwater as constrained by ocean data assimilation, and we aim to demonstrate that we can trust these model transports, through comparison with other independent estimates. The next step is to start to use ocean synthesis products as a data source for understanding changes in water properties and circulation patterns. The ultimate objective is that ocean reanalysis products should become a trusted data source for ocean and climate process-oriented studies, in a similar way that atmospheric reanalyses are currently beginning to be used.

[51] **Acknowledgments.** This work was supported by the *Natural Environment Research Council* (NERC) under the National Centre for Earth Observations (NCEO) and RAPID-Watch Valor programs. Computing resources where provided through the Joint Weather and Climate Research Programme (JWCRP) using the MONSooN (Met Office and NERC Supercomputer Node). Two anonymous reviewers greatly clarified and improved this work.

References

Aagaard, K., and E. C. Carmack (1989), The role of sea ice and other fresh water in the Arctic Circulation, *J. Geophys. Res.*, *94*, 14,485–14,498.

Adcroft, A., C. Hill, and J. Marshall (1997), Representation of topography by shaved cells in a height coordinate ocean model, *Mon. Weather Rev.*, *125*(9), 2293–2315.

Adler, R., G. Huffman, A. Chang, R. Ferraro, P. Xie, J. Janowiak, B. Rudolf, U. Schneider, S. Curtis, and D. Bolvin (2003), The Version-2 Global Precipitation Climatology Project (GPCP) monthly precipitation analysis (1979–present), *J. Hydrometeorol.*, *4*, 1147–1167.

Aoki, K., S. Minobe, Y. Tanimoto, and Y. Sasai (2013), Southward eddy heat transport occurring along Southern Flanks of the Kuroshio extension and the Gulf Stream in a 1/10° global ocean general circulation model, *J. Phys. Oceanogr.*, *43*, 1899–1910, doi:10.1175/JPO-D-12-0223.1.

Barnier, B., et al. (2006), Impact of partial steps and momentum advection schemes in a global ocean circulation model at eddy-permitting resolution, *Ocean Dyn.*, *56*, 6543–6567, doi:10.1007/s10236-006-0082-1.

Bloom, S., L. Takacs, A. DaSilva, and D. Ledvina (1996), Data assimilation using incremental analysis updates, *Mon. Weather Rev.*, *124*, 1256–1271.

Bryden, H. L., and S. Imawaki (2001), Ocean heat transport, in *Ocean Circulation and Climate*, edited by G. Siedler, J. Church, and J. Gould, chap. 6.2, pp. 455–474, Academic Press, London.

Cunningham, S. A., et al. (2007), Temporal variability of the Atlantic meridional overturning circulation at 26.5°N, *Science*, *317*, 935–938.

Dai, A., and K. E. Trenberth (2002), Estimates of freshwater discharge from continents: Latitudinal and seasonal variations, *J. Hydrometeorol.*, *3*(6), 660–687.

Dee, D. P., and S. Uppala (2009), Variational bias correction of satellite radiance data in the ERA-Interim reanalysis, *Q. J. R. Meteorol. Soc.*, *135*, 1830–1841.

Dee, D. P., et al. (2011), The ERA-Interim reanalysis: Configuration and performance of the data assimilation system, *Q. J. R. Meteorol. Soc.*, *137*, 553–597, doi:10.1002/qj.828.

de Vries, P., and S. L. Weber (2005), The Atlantic freshwater budget as a diagnostic for the existence of a stable shut-down of the meridional overturning circulation, *Geophys. Res. Lett.*, *32*, L09606, doi:10.1029/2004GL021450.

Dong, B.-W., and R. T. Sutton (2005), Mechanism of interdecadal Thermohaline Circulation variability in a coupled ocean-atmosphere GCM, *J. Clim.*, *18*, 1117–1135.

Donlon, C. J., M. Martin, J. D. Stark, J. Roberts-Jones, E. Fiedler, and W. Wimmer (2011), The Operational Sea Surface Temperature and Sea Ice analysis (OSTIA), *Remote Sens. Environ.*, *116*, 140–158, doi:10.1016/j.rse.2010.10.017 2011.

Drakkar Group (2007), Eddy permitting ocean circulation hindcasts of past decades, *Clivar Exch. 42*, *12*(3), 8–10.

Drijfhout, S. S., S. L. Weber, and E. van der Swaluw (2010), The stability of the MOC as diagnosed from model projections for pre-industrial, present and future climates, *Clim. Dyn.*, *37*(7–8), 1575–1586, doi:10.1007/s00382-010-0930-z.

Fox, A. D., and K. Haines (2003), Interpretation of Water transformations diagnosed from data assimilation, *J. Phys. Oceanogr.*, *33*, 485–498.

Ganachaud, A., and C. Wunsch (2003), Large scale ocean heat and freshwater transports during the World Ocean Circulation Experiment, *J. Clim.*, *16*, 696–705.

Goosse, H., and T. Fichefet (1999), Importance of ice-ocean interactions for the global ocean circulation: A model study, *J. Geophys. Res.*, *104*, 23,337–23,355.

Haines, K., M. Valdivieso, H. Zuo, and V. N. Stepanov (2012), Transports and budgets in a 1/4° global ocean reanalysis 1989–2010, *Ocean Sci.*, *8*, 333–344, doi:10.5194/os-8-333-2012.

Hartmann, D. (1994), *Global Physical Climatology, International Geophysics*, vol. *56*, edited by Renata Dmowska and James R. Holton, 411 pp., Academic Press, New York.

Hawkins, E., R. S. Smith, L. C. Allison, J. M. Gregory, T. J. Woollings, H. Pohlmann, and B. de Cuevas (2011), Bistability of the Atlantic overturning circulation in a global climate model and links to ocean freshwater transport, *Geophys. Res. Lett.*, *38*, L10605, doi:10.1029/2011GL047208.

Jayne, S. R., and J. Marotzke (2002), The oceanic eddy heat transport, *J. Phys. Oceanogr.*, *32*, 3328–3345.

Large, W., and S. Yeager (2009), The global climatology of an interannually varying air-sea flux data set, *Clim. Dyn.*, *33*, 341–364.

Large, W. G., and S. G. Yeager (2004), Diurnal to decadal global forcing for ocean and sea-ice models: The data sets and flux climatologies, *Tech. Rep. TN-460+STR*, 105 pp., Natl. Cent. for Atmos. Res., Boulder, Colo.

Lea, D. J., J. P. Drecourt, K. Haines, and M. J. Martin (2008), Ocean altimeter assimilation with observational- and model-bias correction, *Q. J. R. Meteorol. Soc.*, *134*(636), 1761–1774.

Lee, T., & Co-Authors (2010), Ocean state estimation for climate research in *Proceedings of OceanObs'09: Sustained Ocean Observations and Information for Society*, vol. *2*, Venice, Italy, 21-25 September 2009, Hall, J., Harrison, D.E. & Stammer, D., Eds., ESA Publication WPP-306, doi:10.5270/OceanObs09.cwp.55.

Levitus, S., J. I. Antonov, T. P. Boyer, R. A. Locarnini, H. E. Garcia, and A. V. Mishonov (2009), Global ocean heat content 1955–2008 in light of recently revealed instrumentation problems, *Geophys. Res. Lett.*, *36*, L07608, doi:10.1029/2008GL037155.

Lique, C., G. Garric, A.-M. Treguier, B. Barnier, N. Ferry, C.-E. Testut, and F. Girard-Ardhuin (2011), Evolution of the Arctic Ocean salinity, 2007–08: Contrast between the Canadian and the Eurasian Basins, *J. Clim.*, *24*, 1705–1717, doi:10.1175/2010JCLI3762.1.

Lorenc, A. C., R. S. Bell, and B. Macpherson (1991), The Meteorological Office analysis correction data assimilation scheme, *Q. J. R. Meteorol. Soc.*, *117*, 59–89, doi:10.1002/qj.49711749704.

Lumpkin, R., and K. Speer (2007), Global ocean meridional overturning, *J. Phys. Oceanogr.*, *37*, 2550–2562, doi:10.1175/JPO3130.1.

Martin, M. J., A. Hines, and M. J. Bell (2007), Data assimilation in the FOAM operational short-range ocean forecasting system: A description of the scheme and its impact, *Q. J. R. Meteorol. Soc.*, *133*, 981–995.

McCann, M. P., A. J. Semtner, and R. M. Chervin (1994), Transports and budgets of volume, heat, and salt from a global eddy-resolving ocean model, *Clim. Dyn.*, *10*, 59–80.

Meijers, A. J., N. L. Bindoff, and J. L. Roberts (2007), On the total, mean, and eddy heat and freshwater transports in the Southern Hemisphere of a 1/8° × 1/8° global ocean model, *J. Phys. Oceanogr.*, *37*(2), 277–295.

Penduff, T., M. Juza, L. Brodeau, G. C. Smith, B. Barnier, J.-M. Molines, A.-M. Treguier, and G. Madec (2010), Impact of global ocean model resolution on sea-level variability with emphasis on interannual time scales, *Ocean Sci.*, *6*, 269–284, doi:10.5194/os-6-269-2010.

Proshutinsky, A., R. H. Bourke, and F. A. McLaughlin (2002), The role of the Beaufort Gyre in Arctic climate variability: Seasonal to decadal climate scales, *Geophys. Res. Lett.*, *29*, 2100, doi:10.1029/2002GL015847.

Reid, J. L. (1994), On the total geostrophic circulation of the North Atlantic Ocean Flow patterns, tracers and transports, *Prog. Oceanogr.*, *33*, 1–92.

Reid, J. L. (1997), On the total geostrophic circulation of the Pacific Ocean; Flow patterns, tracers and transports, *Prog. Oceanogr.*, *39*, 263–352.

Rio, M.-H., P. Schaeffer, J.-M. Lemoine, and F. Hernandez (2005), Estimation of the ocean Mean Dynamic Topography through the combination of altimetric data, in-situ measurements and GRACE geoid: From global to regional studies, paper presented at the GOCINA International Workshop, Luxembourg.

Roberts-Jones, J., E. K. Fiedler, and M. J. Martin (2012), Daily, global, high-resolution SST and sea ice reanalysis for 1985–2007 using the OSTIA system, *J. Clim.*, *25*, 6215–6232, doi:10.1175/JCLI-D-11-00648.1.

Robson, J., R. Sutton, K. Lohmann, D. Smith, and M. D. Palmer (2012), Causes of the rapid warming of the North Atlantic Ocean in the mid-1990s, *J. Clim.*, *25*, 4116–4134, doi:10.1175/JCLI-D-11-00443.1.

Rodwell, M. J., and T. N. Palmer (2007), Using numerical weather prediction to assess climate models, *Q. J. R. Meteorol. Soc.*, *133*, 129–146, doi:10.1002/qj.23.

Roullet, G., and G. Madec (2000), Salt conservation, free surface, and varying levels: A new formulation for ocean general circulation models, *J. Geophys. Res.*, *105*, 23,927–23,942, doi:10.1029/2000JC900089.

Schanze, J. J., R. W. Schmitt, and L. L. Yu (2010), The global oceanic freshwater cycle: A state-of-the-art quantification, *J. Mar. Res.*, *68*, 569–595.

Simmons, A., S. Uppala, D. Dee, and S. Kobayashi (2007), ERA-Interim: New ECMWF reanalysis products from 1989 onwards, *ECMWF Newsl.*, *110*, 25–35.

Smith, R. D., M. E. Maltrud, F. O. Bryan, and M. W. Hecht (2000), Numerical simulation of the North Atlantic Ocean at 1/10°, *J. Phys. Oceanogr.*, *30*, 1532–1561.

Stammer D. (1998), On eddy characteristics, eddy transports, and mean flow properties, *J. Phys. Oceanogr., 28*, 727–739, doi:10.1175/1520-0485(1998)028<0727:OECETA>2.0.CO;2.

Stammer, D., K. Ueyoshi, A. Köhl, W. G. Large, S. A. Josey, and C. Wunsch (2004), Estimating air-sea fluxes of heat, freshwater, and momentum through global ocean data assimilation, *J. Geophys. Res.*, *109*, C05023, doi:10.1029/2003JC002082.

Stammer, D., et al. (2010), Ocean information provided through ensemble ocean syntheses, in *Proceedings of OceanObs–09: Sustained Ocean Observations and Information for Society*, vol. *2*, edited by J. Hall, J., D. E. Harrison and D. Stammer, 21–25 September, Venice, Italy, ESA Publication WPP-306, doi:10.5270/OceanObs09.cwp.85.

Storkey, D., E. W. Blockley, R. Furner, C. Guiavarc'h, D. Lea, M. J. Martin, R. M. Barciela, A. Hines, P. Hyder, and J. R. Siddorn (2010), Forecasting the ocean state using NEMO: The new FOAM system, *J. Oper. Oceanogr.*, *3*, 3–15.

Talley, L. D. (2003), Shallow, intermediate and deep overturning components of the global heat budget, *J. Phys. Oceanogr.*, *33*, 530–560.

Talley, L. D. (2008), Freshwater transport estimates and the global overturning circulation: Shallow, deep and throughflow components, *Prog. Oceanogr.*, *78*, 257–303.

Timmermann, R., H. Goosse, G. Madec, T. Fichefet, C. Ethe, and V. Duliere (2005), On the representation of high latitude processes in the ORCA-LIM global coupled sea ice-ocean model, *Ocean Modell.*, *8*, 175–201.

Treguier, A. M., J. Deshayes, C. Lique, R. Dussin, and J. M. Molines (2012), Eddy contributions to the meridional transport of salt in the North Atlantic, *J. Geophys. Res.*, *117*, C05010, doi:10.1029/2012JC007927.

Trenberth, K. E., J. T. Fasullo, and J. Mackaro (2011), Atmospheric moisture transports from ocean to land and global energy flows in reanalyses, *J. Clim.*, *24*, 4907–4924, doi:10.1175/2011JCLI4171.1.

Valdivieso, M., K. Haines, and H. Zuo (2012), MyOcean Validation Report (ScVR) for V2.1 Reprocessed Analysis and Reanalysis, MyOcean *Tech. Rep. MYO-WP4-GLO-U-Reading_V2.1*, 61 pp., GMES Mar. Core Serv.

Wijffels, S.E. (2001), Ocean transport of freshwater, in *Ocean Circulation and Climate, Int. Geophys. Ser.*, vol. *77*, edited by G. Siedler, J. Church, and J. Gould, pp 475–488, Academic Press, London.

Woodgate, R. A., T. J. Weingartner, and R. Lindsay (2012), Observed increases in Bering Strait oceanic fluxes from the Pacific to the Arctic from 2001 to 2011 and their impacts on the Arctic Ocean water column, *Geophys. Res. Lett.*, *39*, L24603, doi:10.1029/2012GL054092.

Yu, L., X. Jin, and R. A. Weller (2008), Multidecade global flux datasets from the Objectively Analyzed Air-sea Fluxes (OAFlux) Project: Latent and sensible heat fluxes, ocean evaporation, and related surface meteorological variables, *Tech. Rep. OAFlux Project (OA2008-01)*, Woods Hole Oceanogr. Inst.